RGB representation of two-dimensional multi-spectral acoustic data for object surface profile imaging

Xinhua Guo, Yuji Wada, Yosuke Mizuno and Kentaro Nakamura

Precision and Intelligence Laboratory, Tokyo Institute of Technology, 4259 Nagatsuta-cho, Midori-ku, Yokohama 226-8503, Japan

E-mail: guoxinhua@sonic.pi.titech.ac.jp

Abstract

Conventionally, acoustic imaging has been performed using a single frequency or a limited number of frequencies. However, the rich information on surface profiles, structures hidden under surfaces and material properties of objects may exhibit frequency dependence. In this study, acoustic imaging on object surface was conducted over a wide frequency range with a fine frequency step, and a method for displaying the acquired multi-spectral acoustic data was proposed. A complicated rigid surface with different profiles was illuminated by sound waves sweeping over the frequency range from 1 to 20 kHz with a 30 Hz step. The reflected sound was two-dimensionally recorded using a scanning microphone, and processed using a holographic reconstruction method. The two-dimensional distributions of obtained sound pressure at each frequency were defined as 'multi-spectral acoustic imaging data'. Next, the multi-spectral acoustic data were transformed into a single RGB-based picture for easy understanding of the surface characteristics. The acoustic frequencies were allocated to red, green and blue using the RGB filter technique. The depths of the grooves were identified by their colours in the RGB image.

Keywords: frequency dependence, multi-spectral acoustic imaging, acoustic holography, RGB representation

(Some figures may appear in colour only in the online journal)

1. Introduction

As sound waves travel with little attenuation in solids and fluids in which electromagnetic waves do not propagate, acoustic imaging techniques have been applied to many fields including underwater sound navigation and ranging (SONAR) [1–5], medical diagnosis [6–8] and nondestructive evaluation [9–12]. In general, the target object is illuminated by acoustic waves, and then the reflected or transmitted waves are recorded. Finally, the object is visualized by appropriate signal processing.

Acoustic images provide information different from that of optical images, and are significantly influenced by the elastic properties, surface structures, shapes and sizes of the targets to be imaged. These features are reflected in the frequency responses, because frequency-dependent phenomena, such as resonance, diffraction and attenuation, are essentially related to the properties of the objects. On the other hand, use of the optical multi-spectral camera [13, 14], which utilizes spectral information to obtain the detailed characteristics of the objects, has spread recently in research studies on remote sensing and medical tissue diagnostics. As an analogy to multi-spectral imaging in optics, a few studies on the improvement of the quality of images in acoustics with a limited number of frequencies have been reported [15, 16]. For example, for medical purposes, interference noise (speckle) is eliminated by taking average over several images recorded at different frequencies. However, the frequency coverage and resolution in the previous studies are definitely insufficient for the analysis of the resonance characteristics originating from the
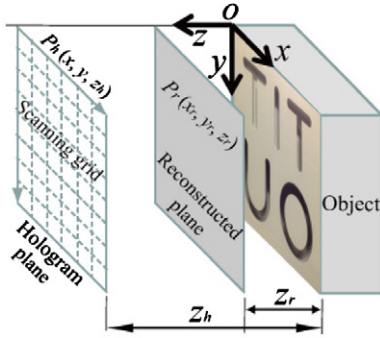
Figure 1. Reconstruction procedure of acoustic holography.

surface profile, because the response changes drastically with the frequency and the higher modes sometimes provide further detailed information.

In this study, to demonstrate the effectiveness of multi-spectral acoustic imaging (MSAI) which utilizes a wide frequency band with a fine frequency step, a complicated sample surface is illuminated by frequency-swept sound from 1 to 20 kHz with a 30 Hz step. We obtain 635 pieces of two-dimensional distributed acoustic images, and each image corresponds to a single frequency. Next, we propose an RGB representation of the measured results as one of the methods for presenting the MSAI data. The acoustic frequencies are allocated to three colours, red (R), green (G) and blue (B), and 635 MSAI images are fused into one picture.

2. Multi-spectral acoustic imaging processing

2.1. Measurement

Multi-spectral acoustic imaging (MSAI) is carried out by measuring the complex sound pressure (amplitude and phase) at each frequency from 1 to 20 kHz with a 30 Hz step. The imaging processing technique based on acoustic holography is used as shown in figure 1. Although impulse response is an alternative method for taking the frequency characteristics, the frequency-swept method is employed in our experiment to enhance the signal-to-noise ratio.

Assuming that the original amplitude and phase data are represented by $a(f, x, y, z_h)$ and $\theta(f, x, y, z_h)$, respectively, where f is the frequency, x and y are the spatial coordinates, and z_h is the constant value that presents the distance between the object surface and the measurement plane, the multi-spectral complex sound pressure is expressed as

$$p_0(f, x, y, z_h) = a(f, x, y, z_h)\, e^{j\theta(f,x,y,z_h)}. \quad (1)$$

To reduce the influence of frequency characteristics of illumination, reflected signals from the surface are calibrated by the reference signal $p_c(f)$. The reference signal $p_c(f)$ is generated as the average of the several selected data $p_0(f, x_i, y_j, z_h)$, where i and j indicate the data positions. The original data contain the phase circulation due to the illumination chirp signal. Before proceeding to the next operation, the phase is compensated using the reference data by the following equation:

$$p_h(f, x, y, z_h) = p_0(f, x, y, z_h)\, e^{-j\arg[p_c(f)]}. \quad (2)$$

2.2. Imaging at every frequency

To visualize the characteristics of object surfaces, planar acoustic holography [17, 18] is applied to the measured sound pressure data. Let us briefly review the procedure to clarify the processing method we employ. The pressure distribution on the surface is derived from the Rayleigh integral equation [19]

$$p_r(f, x_r, y_r, z_r) = \int_{-\infty}^{\infty}\int_{-\infty}^{\infty} p_h(f, x, y, z_h)$$
$$\times g_D(f, x_r - x, y_r - y, z_r - z_h)\, dx_h\, dy_h, \quad (3)$$

where $p_r(f, x_r, y_r, z_r)$ is the multi-spectral complex sound pressure at a point (x_r, y_r, z_r) on the reconstruction plane, $p_h(f, x, y, z_h)$ is the multi-spectral complex sound pressure at a point (x, y, z_h) on the hologram plane and g_D is the Dirichlet Green's function that acts as the transfer function of the sound pressure field from one point to another. The expression of two-dimensional Fourier transforms [19] is employed to treat the sound field in the k-space:

$$\tilde{F}(k_x, k_y) = \int_{-\infty}^{\infty}\int_{-\infty}^{\infty} f(x, y)\, e^{-i(k_x x + k_y y)}\, dx\, dy$$
$$\equiv F[f(x, y)], \quad (4)$$

where (k_x, k_y) refers to the k-space, and (x, y) to the real space. Since (3) is the expression in a two-dimensional convolution integral of $p_h(f, x, y, z_h)$ and $g_D(f, x_r - x, y_r - y, z_r - z_h)$, using the convolution theorem [20, 21], (3) yields

$$p_r(f, x_r, y_r, z_r) = F^-[\tilde{P}_r(k, k_x, k_y, z_r)]$$
$$= F^-[\tilde{P}_h(k, k_x, k_y, z_h)\tilde{G}_D(k, k_x, k_y, z_r - z_h)], \quad (5)$$

where F^- indicates the inverse Fourier transform. This gives the holographic reconstruction of the three-dimensional space $p_r(f, x_r, y_r, z_r)$ in terms of the Fourier transformed form $\tilde{P}_h(k, k_x, k_y, z_h)$ derived from the hologram data $p_h(f, x, y, z_h)$. The operator $\tilde{G}_D(k, k_x, k_y, z_r - z_h)$ is the multi-spectral and two-dimensional spatial Fourier transform of the Dirichlet Green's function.

2.3. RGB representation of the MSAI data

RGB-based colour image, where different colours represent different acoustic frequencies, is a good representation to indicate frequency characteristics at a glance. Three sets of signal data are prepared by using the RGB windows as shown in figure 2. The complex sound pressure p_h is processed through the RGB windows as

$$p_1(x, y, z_h, i) = \sum_{m=1}^{n} w(f_m, i)\, p_h(f_m, x, y, z_h),$$
$$i = [\text{Red, Green, Blue}], \quad (6)$$

where $p_1(x, y, z_h, i)$ is a vector that represents the RGB components of one pixel at (x, y, z_h), and $w(f_m, i)$ represents the RGB windows, f_1 is the lowest frequency, and f_n is the highest frequency for the measurement. In our experiment, $f_1 = 1$ kHz, $f_n = 20$ kHz, $(f_n - f_1)/n = 30$ Hz, and $n = 635$.
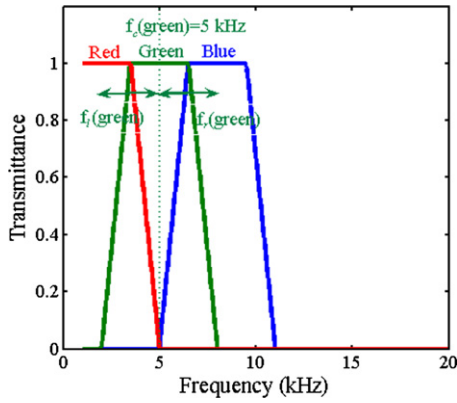
Figure 2. RGB windows.

The trapezoidal windows are given in hue-saturation-value (HSV) [22] colour expression as

$$
w(f, i) = \begin{cases} \dfrac{f - f_l(i)}{f_l(i)/2} & f_c(i) - f_l(i) \leqslant f < f_c(i) - f_l(i)/2 \\ 1 & f_c(i) - f_l(i)/2 \leqslant f < f_c(i) + f_r(i)/2, \\ \dfrac{f_r(i) - f}{fr(i)/2} & f_c(i) + f_r(i)/2 \leqslant f < f_c(i) + f_r(i) \\ 0 & \text{otherwise}. \end{cases}
$$
(7)

where $f_c(i)$, $f_l(i)$ and $f_r(i)$ are the central, the left and the right corner frequencies of the band, respectively. In this study, the trapezoidal windows with the central frequencies of $(R, G, B) = (2, 5, 8)$ kHz are used.

First, the data $p_1(x, y, z_h, i)$ are normalized by the reference value $p_c(i)$ as

$$
p_2(x, y, z_h, i) = \frac{p_1(x, y, z_h, i)}{p_c(i)}.
$$
(8)

Then, the central value is adjusted as the pixel data,

$$
p_3(x, y, z_h, i) = \frac{128|p_2(x, y, z_h, i)| - 128}{3|\sigma(p_2, i)|} + 128,
$$
(9)

where σ is the standard deviation. $P_3(x, y, z_h, i)$ is the magnitude of the RGB representation.

To explore high contrast images, the operation of rotating the phase by parameter φ is applied according to the following procedure:

$$
p_4(x, y, z_h, i) = p_2(x, y, z_h, i) - 1,
$$
(10)

$$
p_5(x, y, z_h, i) = \frac{p_4(x, y, z_h, i)}{3|\sigma(p_4, i)|}.
$$
(11)

The positive real value of the signal $p_5(x, y, z_h, i)$ with phase shift of φ is transformed to the unsigned 8-bit integer for display by the following equations:

$$
p_6(x, y, z_h, i, \varphi) = \text{uint8}\{255 Re[p_5(x, y, z_h, i) e^{j\varphi}]\},
$$
(12)

$$
\text{uint8}(x) = \begin{cases} 255 & (x > 255) \\ 0 & (x < 0) \\ \text{round}(x) & \text{otherwise}. \end{cases}
$$
(13)

3. Experiments

3.1. Sample

A sample for demonstration was a rigid block having a plane surface of 100×100 mm^2 made of polyvinylchloride (PVC). The surface was engraved with five different letters 'T', 'I', 'T', 'U' and 'O' as shown in figure 3(*a*). Here, the upper left 'T' was defined as 'T$_1$', and the upper right 'T' as 'T$_2$'. The five letters formed cavities that were characterized by different geometrical features: all of them had the same width of 6 mm, and differed in depth. The letters 'T$_1$', 'I', 'T$_2$', 'U' and 'O' had depths of 6, 9, 13, 18 and 22 mm, respectively. The other dimensions are indicated in figure 3(*a*). When the cavities were excited by incident waves, every letter exhibited its own resonance frequencies since they had different depths and shapes.

3.2. Experimental set-up and data acquisition

The experimental set-up is shown in figure 3(*b*). A loudspeaker (Fostex, T90A) and a needle microphone (B&K, 4182) were mounted on the X–Y motorized stage, and moved along the hologram plane parallel to the sample surface. The distance from the microphone to the sample surface was 2 mm, and
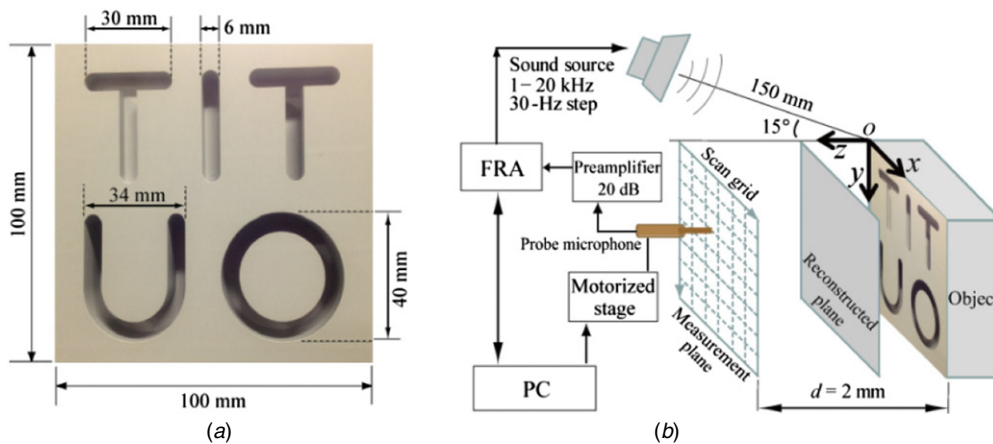

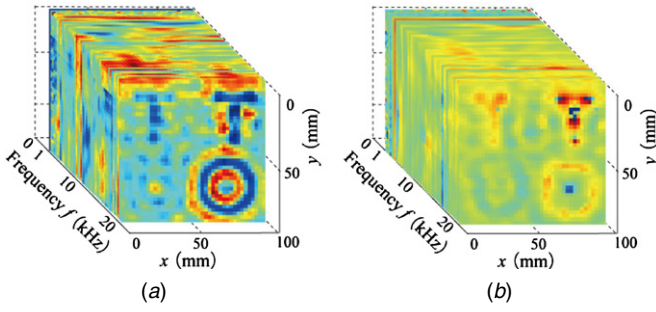**Figure 3.** (*a*) Sample with the detailed dimensions (optical image), and (*b*) experimental set-up.

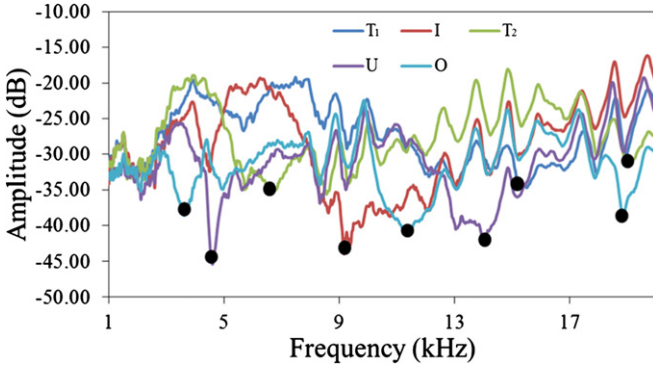**Figure 4.** (*a*) Amplitude and (*b*) phase distributions (MSAI data).

Figure 5. Frequency responses for five letters.

from the loudspeaker to the sample surface was 150 mm. The incident angle was 15 degrees. The continuous sound wave (linear chirp signal) was radiated onto the object surface. The reflected sound was detected using the needle microphone that had smooth frequency response characteristic between 1 Hz and 20 kHz. At every microphone position (*x*, *y*), the loudspeaker transmitted a frequency-swept sound from 1 to 20 kHz with a step of 30 Hz. Using a frequency response analyzer (FRA, NF5097), the received data of the amplitude and phase at each frequency was transferred to a personal computer (PC) for further processing. The signal source driving the loudspeaker was generated by the same FRA, and was used as the reference signal for determining the phase of the sound pressure. The *X*–*Y* scanning points were 40 × 40, and the grid spacing was 2.5 mm. The time required for data acquisition was 12 h for all the measurement and preprocessing.

After the measurement was completed, acquired data were arranged into two-dimensional distributions of the amplitude and phase at each frequency as shown in figure 4. We had acoustic holograms at every 30 Hz from 1 to 20 kHz, thus the total number of obtained holograms was 635. These were recognized as the MSAI data. In this example, six points in the data (*x*, *y*) = (15, 10), (25, 10), (10, 20), (20, 20), (30, 20), (20, 30) were selected for the calibration stated in section 2.1.
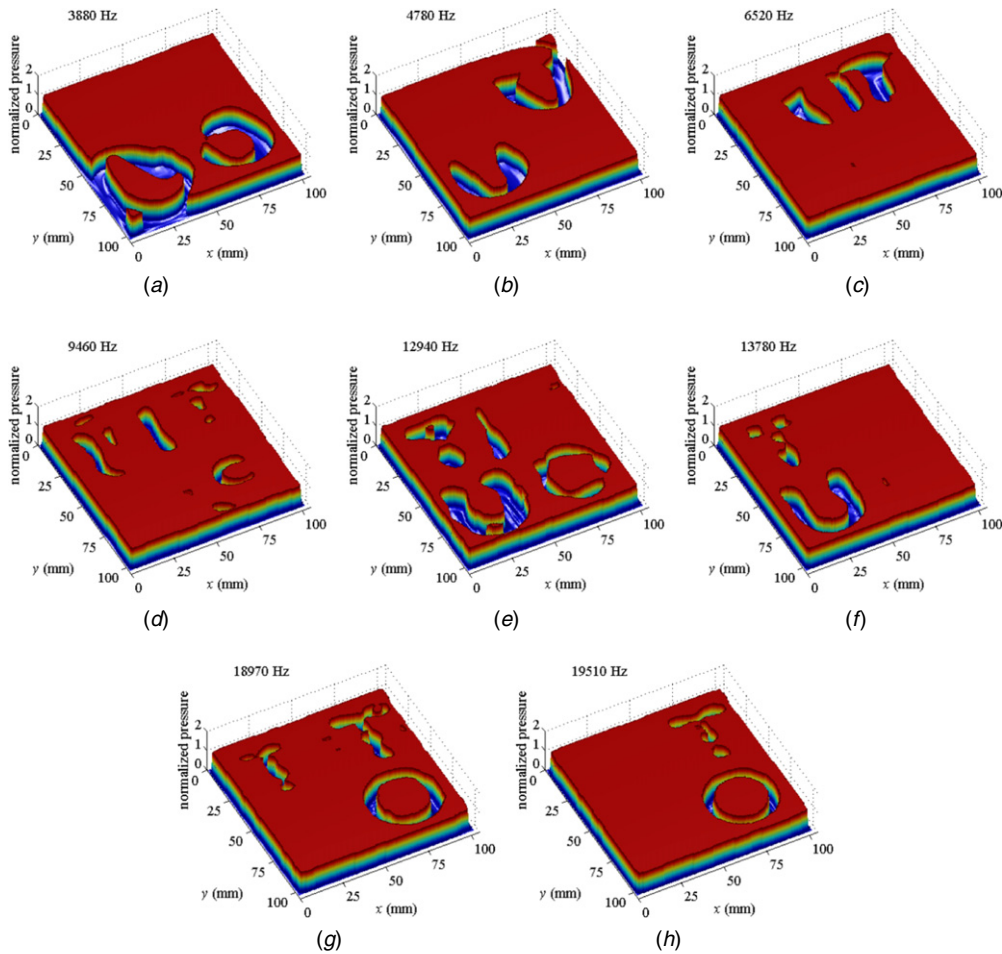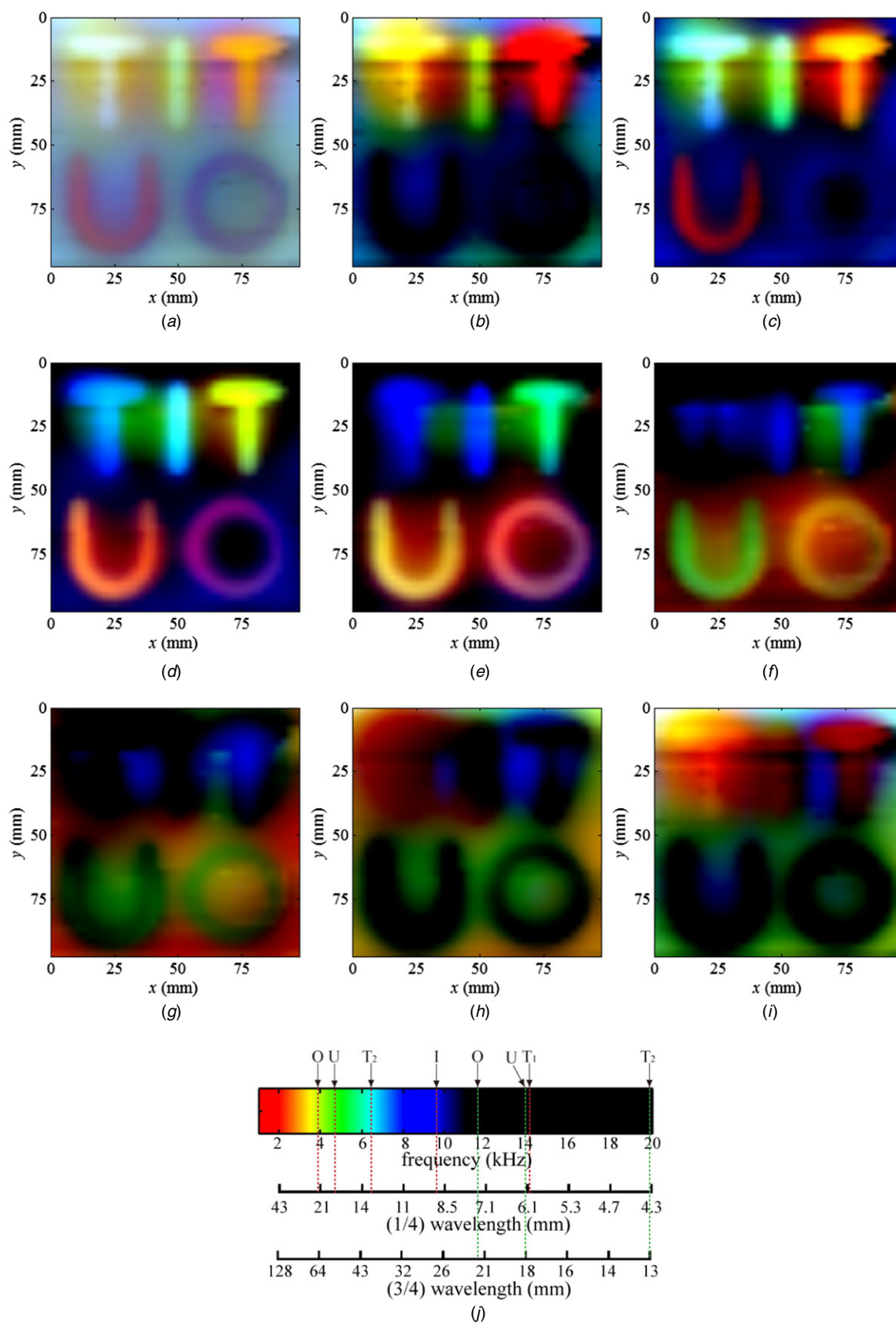

Figure 6. (*a*)–(*h*) Reconstructed images at different frequencies of the object surface.

Figure 7. (*a*) Amplitude, (*b*)–(*i*) RGB representations with rotating phases $\varphi = 0$, $\pi/4$, $\pi/2$, $3\pi/4$, π, $5\pi/4$, $3\pi/2$ and $7\pi/4$, respectively, and (*j*) colour bar.

4. Results

4.1. Basic frequency responses

Since the frequency responses varied by the position along one letter, mean frequency responses of each letter were used for simplicity. The mean values were calculated from the measured points located along the letters. For focusing on the resonance of depth mode, the characteristics of the mean frequency responses for each letter are shown in figure 5. The fundamental, second and third harmonics of the letter 'O' were observed, while the fundamental and second harmonics of the 'U' and 'T$_2$', and the fundamental harmonic of the letters 'I' and 'T$_1$' were found.

According to the theory for a one-dimensional closed end tube, resonating at the odd harmonics, i.e. $\lambda/4$, $3\lambda/4$, $5\lambda/4$, $7\lambda/4, \ldots$, and $n \cdot \lambda/4$ (λ represents the sound wavelength, and n denotes the odd integers), the resonant frequencies for the different depths of the letters (TITUO) were calculated to be 14.2, 9.4, 6.5, 4.7 and 3.9 kHz, corresponding to the depths of 6, 9, 13, 18 and 22 mm, respectively. The measured resonant frequencies were 15.1, 9.1, 6.3, 4.5 and 3.5 kHz as shown in figure 5. Although there were errors in the results, the depths of the letters were roughly identified by the mean frequency to some extent. For more precise estimation, three-dimensional discussion about the acoustic resonance of cavity is required.

4.2. Imaging at each frequency

All 635 holograms from 1 to 20 kHz with a 30 Hz step were reconstructed by the form of the Rayleigh integral expressed in (5). Eight reconstructed images of the magnitude of sound pressure were picked up from the 635 images and are shown in figures 6(*a*)–(*h*). With increasing frequency, the five letters 'TITUO' engraved in the surface showed different responses. The deepest letter 'O' responded at the lowest frequency as shown in figure 6(*a*), and the second and the higher harmonics were observed in figures 6(*e*), (*g*) and (*h*), respectively. The letter 'U' was observed at the fundamental resonant frequency in figure 6(*b*) and the second harmonic in figures 6(*e*) and (*f*). 'T$_2$' was seen at the fundamental resonant frequency in figure 6(*c*) and the second harmonic in figures 6(*g*) and (*h*). The letters 'I' and 'T$_1$' were observed in figures 6(*d*) and (*f*), respectively. Although it was difficult to discriminate 'T$_1$' from 'T$_2$' using the optical images, they were easily recognized by the MSAI technique. The letters 'T$_1$' and 'T$_2$' were not observed at the same frequencies of 12 940, 13 780 and 19 510 Hz in figures 6(*e*), (*f*) and (*h*). However, both 'T$_1$' and 'T$_2$' were observed at the same frequency of 18 970 Hz as shown in figure 6(*g*). In addition, the responses of the four letters were observed at the frequency of 12 940 Hz except for the letter 'T$_2$' as shown in figure 6(*e*). These results indicated that the surface profiles of the object were seen by their own acoustic spectral characteristics.

4.3. RGB representation

Based on the transformation using the RGB filters, the MSAI data, all the frequency characteristics of the surface profiles, were fused into one RGB image. The amplitude result is shown in figure 7(*a*). The five letters were clearly observed and had different frequency responses displayed by different colours. To explore higher contrast of the images, RGB images with various phases, $\varphi = 0$, $\pi/4$, $\pi/2$, $3\pi/4$, π, $5\pi/4$, $3\pi/2$ and $7\pi/4$, were created as shown in figures 7(*b*)–(*i*). The case for $\varphi = \pi/2$ showed the high contrast image as shown in figure 7(*d*). The frequency characteristics of each letter were successfully observed in one picture using the RGB representation. Figure 7(*j*) shows the colour bar and the corresponding acoustic frequency. The wavelengths for 1/4- and 3/4-wavelength resonances of a one-dimensional single-end tube are also displayed in the figure. Based on the colour bar corresponding to the frequency band, we roughly estimated which grooves were the deepest and the shallowest. The grooves of the letters 'T$_1$', 'I', 'T$_2$', 'U' and 'O' corresponded to blue, deep sky-blue, yellow, coral and fuchsia, respectively, which meant that the groove of the letter 'T$_1$' was the shallowest one with the highest resonant frequency, and the groove of the letter 'O' was the deepest. In addition, it was observed that the distribution of the colour in each letter was not even. This was probably affected by the horizontal acoustic mode in the grooves. The letter 'O' had the second harmonic at 8–10 kHz, thus the letter 'O' was displayed by two mixed colours.

5. Conclusions

The effectiveness of the MSAI was demonstrated using a wide frequency band from 1–20 kHz with a fine frequency step of 30 Hz. To understand the surface profile using one picture, the RGB representation was proposed. The images of letters 'TITUO' engraved on a rigid surface were observed at each frequency by acoustic holography. The different structures of the surface were distinguished by the characteristics of their acoustic frequency responses. It was verified that the multi-spectral imaging was also a powerful tool in acoustics, and gave us different information from optical imaging.

The typical trapezoidal RGB windows were employed in this study for the RGB representation. Different designs of the RGB windows may result in different images. The central frequencies of the RGB windows should be selected according to the applications. We should note that, in the RGB representation, only a part of the rich information involved in the MSAI data is displayed, and the rest of the information is lost.

References

[1] Wallace R H, Hillery H V, Barnard G R, Marks B M and McKinney C M 1975 Experimental investigation of several passive sonar targets *J. Acoust. Soc. Am.* **57** 862–9

[2] Capéran T, Hayward G and Chapman R 1999 A 3D simulator for the design and evaluation of sonar system instrumentation *Meas. Sci. Technol.* **10** 1116–26

[3] Iwata T, Goto Y and Susaki H 2001 Application of the multiple signal classification (MUSIC) method for one-pulse burst-echo Doppler sonar data *Meas. Sci. Technol.* **12** 2178–84

[4] Hickman G and Krolik J L 2004 Matched-field depth estimation for active sonar *J. Acoust. Soc. Am.* **115** 620–9

[5] Nakahira K, Kodama T, Furuhashi T and Okuma S 2004 A self-adapting sonar ranging system based on digital polarity correlators *Meas. Sci. Technol.* **15** 347–52

[6] Chivers R C and Parry R J 1978 Ultrasonic velocity and attenuation in mammalian tissues *J. Acoust. Soc. Am.* **63** 940–53

[7] Nock L, Trahey G E and Smith S W 1989 Phase aberration correction in medical ultrasound using speckle brightness as a quality factor *J. Acoust. Soc. Am.* **85** 1819–33

[8] Hinkelman L M, Liu D L, Waag R C, Zhu Q and Steinberg B D 1995 Measurement and correction of ultrasonic pulse distortion produced by the human breast *J. Acoust. Soc. Am.* **97** 1958–69

[9] Chen E P 1977 Impact response of a layered composite containing a crack *J. Acoust. Soc. Am.* **61** 727–30

[10] Han X, Favro L D and Thomas R L 2011 Sonic IR imaging of delaminations and disbonds in composites *J. Phys. D: Appl. Phys.* **44** 034013

[11] Bowler N 2011 Four-point potential drop measurements for materials characterization *Meas. Sci. Technol.* **22** 012001

[12] Mitri F G, Kinnick R R, Greenleaf J F and Fatemi M 2009 Continuous-wave ultrasound reflectometry for surface roughness imaging applications *Ultrasonics* **49** 10–4

[13] Sakanoi T, Okano S, Obuchi Y, Kobayashi T, Ejiri M, Asamura K and Hirahara M 2003 Development of the multi-spectral auroral camera onboard the index satellite *Adv. Space Res.* **32** 379–84

[14] Basiri A, Nabili M, Mathews S, Libin A, Groah S, Noordmans H J and Ramella-Roman J C 2010 Use of a multi-spectral camera in the characterization of skin wounds *Opt. Express* **18** 3244–57

[15] Yoshizumi N, Saito S, Koyama D, Nakamura K, Ohya A and Akiyama I 2009 Multiple-frequency ultrasonic imaging by transmitting pulsed waves of two frequencies *J. Med. Ultrason.* **36** 53–60

[16] Akiyama I, Yoshizumi N, Saito S, Wada Y, Koyama D and Nakamura K 2012 Development of multiple-frequency ultrasonic imaging system using multiple resonance piezoelectric transducer *Japan. J. Appl. Phys.* **51** 07GF02

[17] Maynard J D, Williams E G and Lee Y 1985 Nearfield acoustical holography: I. Theory of generalized holography and the development of NAH *J. Acoust. Soc. Am.* **78** 1395–413

[18] Veronesi W A and Maynard J D 1987 Nearfield acoustic holography (NAH) II. Holographic reconstruction algorithms and computer implementation *J. Acoust. Soc. Am.* **81** 1307–22

[19] Williams E G 1999 *Fourier Acoustics—Sound Radiation and Nearfield Acoustical Holography* (San Diego, CA: Academic) pp 31–5

[20] Goodman J W 1968 *Introduction to Fourier Optics* (New York: McGraw-Hill) p 10

[21] Williams E G 1999 *Fourier Acoustics—Sound Radiation and Nearfield Acoustical Holography* (San Diego, CA: Academic) p 3

[22] Smith A R 1978 Color gamut transform pairs *Comput. Graph.* **12** 12–9